Bull. Mater. Sci., Vol. 39, No. 3, June 2016, pp. 827–835. © Indian Academy of Sciences.
DOI 10.1007/s12034-016-1189-8

Ab initio calculations of fundamental properties of $SrTe_{1-x}O_x$ alloys

J ZEROUAL[1], S LABIDI[1], H MERADJI[2,*], M LABIDI[1] and F EL HAJ HASSAN[3]

[1]Department of Physics, Faculty of Sciences, Badji Mokhtar University, P.O. Box 12, 23000 Annaba, Algeria
[2]Laboratoire LPR, Département de Physique, Faculté des Sciences, Université Badji Mokhtar, Annaba, Algeria
[3]Laboratoire de Physique et d'électronique (LPE), Faculté des Sciences, Université Libanaise, El Hadath, Beirut, Lebanon

MS received 18 April 2015; accepted 24 November 2015

Abstract. **Structural, electronic, optical and thermodynamic properties of the $SrTe_{1-x}O_x$ alloys ($0 \leq x \leq 1$) in rock-salt phase are calculated using the full potential-linearized augmented plane wave (FP-LAPW) method within density functional theory. The exchange-correlation potential for structural properties was calculated by the standard local density approximation (LDA) and GGA (PBE) and the new form of GGA (WC) which is an improved form of the most popular Perdew–Burke–Ernzerhof (PBE), while for electronic properties, in addition to LDA, GGA corrections; Engel–Vosko GGA (EV-GGA) and modified Becke–Johnson (mBJ) schemes were also applied. The results show that the use of GGA (WC) in our calculations is more appropriate than GGA and LDA and gives a good description of structural properties such as lattice parameters and bulk modulus. Our investigation on the effect of composition on lattice constant, bulk modulus and band gap for ternary alloys shows almost nonlinear dependence on the composition. In addition to FP-LAPW method, the composition dependence of the refractive index and the dielectric constant was studied by different models. On the other hand, the thermodynamic stability of this alloy was investigated by calculating the excess enthalpy of mixing ΔH_m as well as the phase diagram.**

Keywords. **Alloys; *ab initio* calculations; electronic properties; DFT.**

1. Introduction

Strontium telluride, SrTe, like other alkaline-earth tellurides has recently attracted significant attention of researchers because of its potential technological applications ranging from catalysis to microelectronics and optoelectronics [1–4]. SrTe is an important closed-shell ionic compound, which crystallizes in NaCl-type (B1) structure at ambient conditions. However, high pressure X-ray diffraction experiment has shown that on applying pressure up to about (12 ± 1) GPa, SrTe undergoes a structural phase transition to CsCl-type (B2) structure with a relative volume collapse of $(11.1 \pm 0.7)\%$ [5]. Therefore, various theoretical calculations have been performed to study the structural, electronic and mechanical properties of SrTe; Khenata *et al* [6] calculated electronic band structures and total energies of SrS, SrSe and SrTe in NaCl and CsCl-type structures using full potential–linearized augmented plane wave method (FP-LAPW) within the generalized gradient approximation (GGA). Shameen Banu *et al* [7] also reported similar results using the tight binding linear muffin-tin orbital method within the framework of local density approximation (LDA). Moreover, Cortona [8] have discussed the cohesive properties and the behaviour under pressure of SrSe and SrTe by *ab initio* method that allows the direct determination of the electron density and the total energy of a system in the framework of the density-functional theory. Rached *et al* [9] have mentioned the stability criteria of these compounds and reported second-order elastic constant using first principles calculations. Earlier, the elastic constants are investigated using pseudopotential [10] and tight binding methods [11].

Recently, Liwei Shi *et al* [12] reported first-principles pseudopotential calculations of the structural, electronic, elastic and optical properties as well as phase transition under pressure of SrTe.

The second compound of the present work, cubic strontium oxide (SrO) also has technological importance in the manufacture of electronic devices, such as important constituents of earth's lower mantle where pressure reaches up to 140 GPa. The electronic structure of this compound inside the earth will be considerably changed compared to that at normal pressure. So SrO is of geophysical interest [13–17]. At normal conditions, this compound crystallizes in the NaCl-type (B1) structure (Fm3m) and have both properties of ordinary insulators with a wide band gap [18] of $E_g = 5.727$ eV and properties of semiconductors with large valence bandwidth of $E_v > 60$ eV.

As the alloy system between SrTe and SrO has never been investigated, the purpose of this paper is to study the structural, electronic, optical and thermodynamic properties of $SrTe_{1-x}O_x$. In semiconductor alloys, the band gap value and the lattice parameter are among the most important physical parameters, since these parameters control the band offset and the mismatching in the different devices. The lattice parameter of the ternary alloy $SrTe_{1-x}O_x$ is well described

*Author for correspondence (hmeradji@yahoo.fr)

by Vegard's law [19], but this is not the case of the band gap value. To help, understand and control the material and behaviour of bowing and related properties, we have investigated the effect of the O concentration on the structural, electronic and optical properties of the $SrTe_{1-x}O_x$ alloys with O contents between 0 and 1 using the full potential-linearized augmented plane wave (FP-LAPW) method. Various quantities, including lattice parameters, bulk modulus, band gap, refractive index and the thermodynamic stability were obtained for this alloy.

The paper is described as follows. In the following section, the computational method used in the present work is described. Section 3 is devoted to the presentation of results and discussion for structural, electronic, bowing parameters, optical and thermodynamic properties. Finally, in section 4, a brief summary is given.

2. Method of calculations

Describing random alloys by periodic structures will clearly introduce spurious correlations beyond a certain distance ('periodicity errors'). Preventing this problem needs a very large supercell. However, many physical properties of solids are characterized by microscopic length scales and local randomness of alloys and modifying the large scale randomness of alloys does not affect them. Zunger *et al* [20] implemented this fact to construct 'special quasirandom structures' (SQS) approach by the principle of close reproduction of the perfectly random network for the first few shells around a given site, deferring periodicity errors to more distant neighbours. They argued that this approach, which we have adopted in our calculation, effectively reduces the size of the supercell to study many properties of random alloys.

The calculations were performed using the full-potential linear augmented plane wave (FP-LAPW) method within the framework of density functional theory (DFT) [21,22] as implemented in the wien2k code [23]. For structural properties, the exchange-correlation potential was calculated using the LDA [24], GGA (PBE) [25] and the new form of GGA (WC-GGA) [26] which is an improved form of the most popular Perdew–Burke–Ernzerhof (PBE-GGA), while for electronic properties, in addition to LDA and PBE-GGA corrections, the Engel–Vosko GGA (EV-GGA) [27] and the modified Becke–Johnson (mBJ) [28,29] schemes were also applied. In the FP-LAPW method, the wave function, charge density and potential are expanded differently in the two regions of unit cell. Inside the non-overlapping spheres of radius R_{MT} around each atom, a spherical harmonics expansion is used,

$$V(r) = \sum_{lm} V_{lm}(r)\, Y_{lm}\left(\hat{r}\right), \tag{1}$$

and outside the sphere (interstitial region), a plane wave basis set is chosen,

$$V(r) = \sum_{k} V_k e^{ikr}, \tag{2}$$

where $Y_{lm}\left(\hat{r}\right)$ is a linear combination of radial functions times spherical harmonics. Within this calculational scheme, there are no shape approximations to the charge density or potential. In the present calculation, a cubic super cell that is composed of eight atoms (four Sr atoms and four shared out between Te and O) is considered. We use a parameter $R_{MT}K_{max} = 8$ which determines the matrix size, where R_{MT} denotes the smallest atomic sphere radius and K_{max} gives the magnitude of the largest K vector in the plane wave expansion. The charge density was Fourier expanded up to $G_{max} = 14\ (Ryd)^{1/2}$. The maximum l values for the wave function expansion inside the spheres was confined to $l_{max} = 10$. We chose the muffin-tin radius of Sr, Te and O to be 2.2, 2.4 and 2.1 au, respectively. A mesh of 47 special k-points for binary compounds and 125 special k-points for alloys were taken in the irreducible wedge of the Brillouin zone for the total energy calculation. Both the plane wave cut-off and the number of k-points were varied to ensure total energy convergence.

3. Results and discussion

3.1 *Structural properties*

The ground state bulk properties of the crystals were obtained using the calculations of the total energy as a function of unit cell volume. Our calculated values for the equilibrium lattice constant a and the bulk modulus B for $SrTe_{1-x}O_x$ alloy $0 \leq x \leq 1$ using three approximations, WC-GGA, PBE-GGA and LDA are summarized in table 1 together with the available experimental and theoretical data. It is found that the calculated equilibrium lattice constants for SrTe and SrO using WC-GGA functional are in agreement with the experiments [5,30], whereas LDA and PBE-GGA underestimate and overestimate these values, respectively. Similarly, the bulk modulus B for SrTe and SrO, as calculated by the WC-GGA are in good agreement with the experimental results [5,30].

The calculated equilibrium lattice constants *vs.* concentration of alloys have been plotted against concentration x in figure 1. A large deviation from Vegard's law with an upward bowing parameters equal to −0.946, −0.930 and −0.880 Å with WC-GGA, PBE-GGA and LDA, respectively, obtained by fitting the calculated values with a polynomial function was observed. The physical origin of this deviation could be mainly due to the atomic radii difference of Te (1.4 Å) and O (0.6 Å) atoms. Our results indicate that this violation of Vegard's law has a significant effect on the optical bowing parameter as shown in the next section.

Figure 2 shows the bulk modulus as a function of x for the $SrTe_{1-x}O_x$ alloys. A significant deviation from the linear concentration dependence (LCD) with downward bowing equal to 87.20, 93.94 and 86.85 GPa with WC-GGA, PBE-GGA and LDA, respectively, was observed. The physical origin of this deviation should be mainly due to the mismatches of the bulk modulus of the binary compounds.

Table 1. The optimized lattice constants (a(Å)) and bulk modules (B (GPa)) calculated by different exchange-correlation energy approximations for $SrTe_{1-x}O_x$ $0 \leq x \leq 1$.

	Lattice constant a (Å)					Bulk modulus B (GPa)				
	This work					This work				
x	LDA	GGA	WC	Exp.	Other work	LDA	GGA	WC	Exp.	Other work
0	6.527	6.735	6.612	6.66[a]	6.76[c], 6.531[d]	39.0	31.8	35.9	39.5[a]	36[c], 39.1[d], 65.41848[f]
0.25	6.305	6.485	6.389			43.6	32.9	38.3		
0.50	6.018	6.204	6.100			50.6	37.0	45.3		
0.75	5.626	5.793	5.703			65.9	51.1	57.0		
1	5.071	5.201	5.120	5.16[b]	5.073[e]	104.2	88.3	95.2	91[b]	105[e], 143.89[f]

[a]Ref [5]; [b]ref [30]; [c]ref [6]; [d]ref [12]; [e]ref [31]; [f]ref [30].

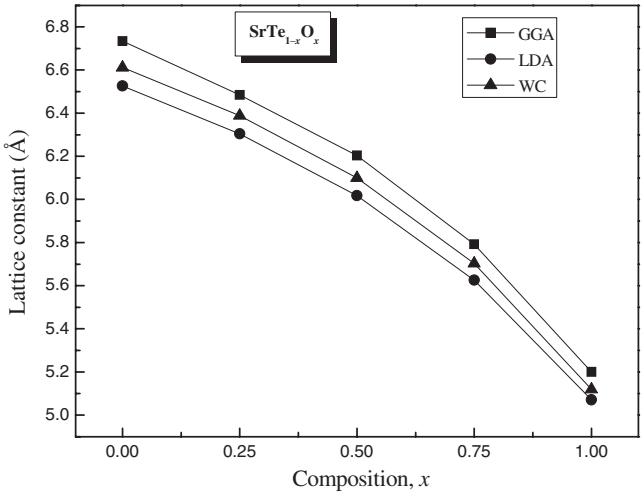

Figure 1. Concentration dependence of the lattice constants calculated by different exchange-correlation energy approximations for $SrTe_{1-x}O_x$ alloy.

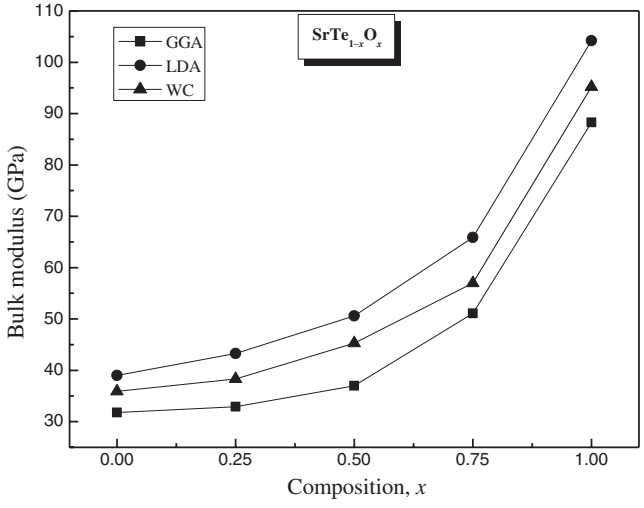

Figure 2. Concentration dependence of the bulk modulus calculated by different exchange-correlation energy approximations for $SrTe_{1-x}O_x$ alloy.

Our results show that the bulk modulus increases with an increase in the O concentration x. This suggests that as x increases from $x = 0$ to 1, the alloys become generally less compressible.

A more precise comparison of behaviour of the lattice constant and bulk modulus of the ternary alloys shows that a decrease of the earlier parameter is accompanied by an increase of the latter one and vice versa. It represents bond strengthening or weakening effects induced by changing the composition.

3.2 *Electronic properties*

3.2a *Band structures*: Knowledge of the energy band structures provides valuable information regarding its potential utility in manufacture of the electronic devices. It is also well known that in the electronic band structure calculations within DFT, both LDA and GGA usually underestimate the energy band gap compared to the experimental one [32]. This is mainly due to the fact that they have simple forms that are not sufficiently flexible to accurately reproduce both the exchange-correlation energy and its charge derivative. Here, we have tried the EV-GGA and mBJ along with the standard LDA and PBE-GGA for the band structure calculations.

Calculated results for the band gaps of SrTe, SrO and their alloy using LDA, PBE-GGA and EV-GGA, are summarized in table 2, along with the available experimental values and those obtained by earlier theoretical calculations for the binary compounds, but in the case of alloys, there is no theoretical and experiment value to compare with. The mBJ band gap value of the binary compound SrO is close to the experiment, which is a support for those of the ternary alloys. According to current calculations, mBJ performed better than other conventional DFT functionals to calculate band structure. For this reason, mBJ is a very effective method for electronic properties and it can be used for a wide range of semiconductors.

It shows that the results calculated by EV-GGA are reasonably in agreement with experiment; LDA and PBE-GGA give lower values. EV-GGA reproduces better exchange potential at the cost of less accuracy in exchange energy. Owing to this reason EV-GGA presents better results for

Table 2. The energy gaps (in eV) calculated by different exchange-correlation energy approximations for $SrTe_{1-x}O_x$ $0 \leq x \leq 1$.

	E_g (eV)					
	This work					
x	LDA	GGA	EV-GGA	mBJ	Exp.	Other work
0	1.443	1.807	2.554	2.489	4.32[a]	1.73[b], 1.89[c]
0.25	1.324	1.373	1.751	1.749		
0.50	1.425	1.479	1.651	1.898		
0.75	2.018	2.234	2.686	3.118		
1	3.125	3.334	4.032	5.142	5.727[a]	3.391[d], 3.01[e]

[a]Ref [18]; [b]ref [5]; [c]ref [33]; [d]ref [34]; [e]ref [31].

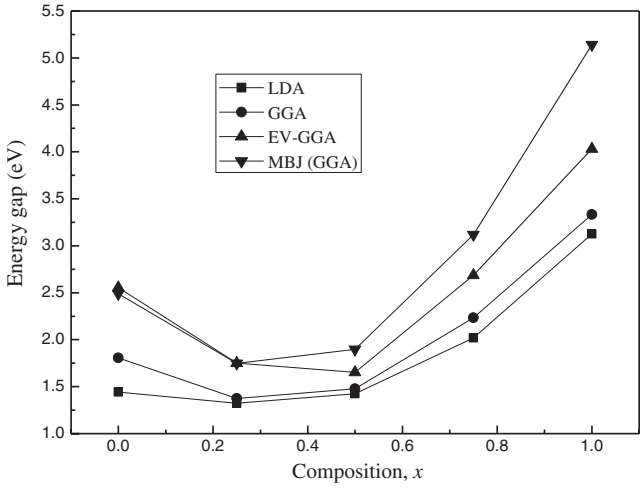

Figure 3. Band-gap energies of the $SrTe_{1-x}O_x$ alloys as a function of O concentrations using LDA, GGA, EV-GGA and mBJ.

band gap energy and other properties which depend primarily on exchange potential.

Figure 3 shows the composition dependence of the calculated band gaps using LDA, PBE-GGA and EV-GGA schemes. It is clearly seen that the energy gap shows a nonlinear variation with concentration x, providing a positive gap bowing. We calculated the total bowing parameter by fitting the nonlinear variation of calculated band gaps *vs.* concentration with quadratic function. The results obey the following variations:

$$SrTe_{1-x}O_x \Rightarrow \begin{cases} E_g^{LDA}(x) = 1.475 - 1.741x + 3.364x^2 \\ E_g^{GGA}(x) = 1.793 - 2.682x + 4.248x^2 \\ E_g^{EVGGA}(x) = 2.532 - 4.652x + 6.209x^2 \\ E_g^{mBJ}(x) = 2.486 - 4.871x + 7.541x^2 \end{cases} \quad (3)$$

To obtain the origins of bowing parameter (b), we adopted the approach of Zunger and co-workers [35]. According to this approach, gap bowing coefficient (b) is assumed to be independent of composition x and is decomposed into three physically distinct contributions. The overall gap bowing coefficient at $x = 0.5$, measures the change in band gap according to the equation:

$$AB(a_{AB}) + AC(a_{AC}) \rightarrow AB_{0.5}C_{0.5}(a_{eq}), \quad (4)$$

where a_{AB} and a_{AC} are the equilibrium lattice constants of the binary compounds AB and AC, respectively, and a_{eq} the alloy equilibrium lattice constant. We now decompose equation (4) into three steps:

$$AB(a_{AB}) + AC(a_{AC}) \xrightarrow{VD} AB(a) + AC(a), \quad (5)$$

$$AB(a) + AC(a) \xrightarrow{CE} AB_{0.5}C_{0.5}(a), \quad (6)$$

$$AB_{0.5}C_{0.5}(a) \xrightarrow{SR} AB_{0.5}C_{0.5}(a_{eq}). \quad (7)$$

The first step measures the effect of volume deformation (VD) on the energy gap bowing. The corresponding contribution b_{VD} to the total gap bowing parameter represents the relative response of the band structure of the binary compounds AB and AC to hydrostatic pressure. This is due to the change of their individual equilibrium lattice constants to the alloy value $a = a(x)$ (from Vegard's rule). The second step due to the charge-exchange (CE) contribution b_{CE} reflects a charge-transfer effect that is due to the different (averaged) bonding behaviour at the lattice constant a. The final step measures changes due to the structural relaxation (SR) in passing from the unrelaxed to the relaxed alloy by b_{SR}.

Consequently, the total gap bowing parameter is defined as:

$$b = b_{VD} + b_{CE} + b_{SR}, \quad (8)$$

$$b_{VD} = 2\left[\varepsilon_{AB}(a_{AB}) - \varepsilon_{AB}(a) + \varepsilon_{AC}(a_{AC}) - \varepsilon_{AC}(a)\right], \quad (9)$$

$$b_{CE} = 2\left[\varepsilon_{AB}(a) + \varepsilon_{AC}(a) - 2\varepsilon_{ABc}(a)\right], \quad (10)$$

$$b_{SR} = 4\left[\varepsilon_{ABC}(a) - 2\varepsilon_{ABc}(a_{eq})\right], \quad (11)$$

where ε is the energy gap which has been calculated for the indicated atomic structures and lattice constants. The energy gap terms in equations (9)–(11) are calculated separately with a self-consistent band structure approach FP-LAPW. The results are given in table 3. We note that the calculated quadratic parameters (gap bowing) within LDA, PBE-GGA, EVGGA and mBJ are very close to their corresponding results obtained by the Zunger's approach. We conclude that the main contribution to the gap bowing is raised from the volume deformation effect. This can be clearly attributed to the large mismatch of the lattice constants of the corresponding binary compounds. The charge transfer contribution b_{CE} is also significant. It is due to the large electronegativity difference between Te (2.1) and O (3.44) atoms. The contribution of the structural relaxation b_{SR} is small. Finally, it is clearly seen that our EV-GGA value for bowing parameter are larger than the corresponding value within PBE-GGA, LDA and mBJ.

Table 3. Decomposition of the optical bowing into volume deformation (VD), charge exchange (CE) and structural relaxation (SR) contributions compared with that obtained by a quadratic fit (all values are in eV).

		This work							
		Zunger approach				Quadratic fits			
		LDA	GGA	EV-GGA	mBJ	LDA	GGA	EV-GGA	mBJ
$SrTe_{1-x}O_x$	b_{VD}	2.493	5.289	5.739	4.09				
	b_{CE}	2.209	−0.518	0.426	3.72				
	b_{SR}	−1.267	−0.406	0.403	−0.108				
	b	3.436	4.366	6.568	7.702	3.364	4.248	6.209	7.541

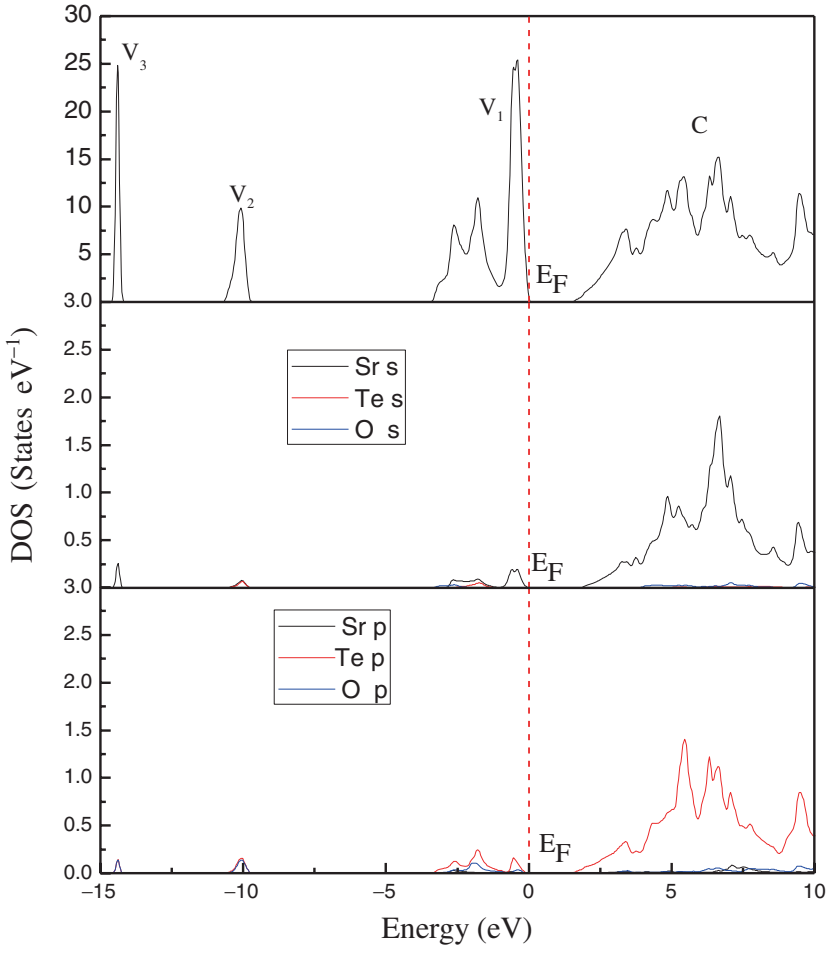

Figure 4. Total density of states (TDOS) and partial density of states (PDOS) of $SrTe_{0.5}O_{0.5}$ alloy.

3.2b *Densities of states*: Due to the close similarity between the results obtained for these $SrTe_{1-x}O_x$ alloys, the density of states (DOS) is only given for the $SrTe_{0.5}O_{0.5}$ alloy as prototype. The calculated total density of states (TDOS) and partial density of states (PDOS) for the $SrTe_{0.5}O_{0.5}$ alloy in the energy range between −15 and 10 eV using PBE-GGA approximation are illustrated in figure 4. For $SrTe_{0.5}O_{0.5}$, three groups of valence bands were observed. The upper group of valence bands V_1 occupies the energy range of 0 to −3.55. It is formed by hybridization between Sr-s states and Te-p states. The second group V_2 immediately below the upper group V_1 consists of p (Te, O) states, with little contribution from Te-s states. The third one V_3 is formed emanating from hybridization between Sr-s and O-p states. The bottom of the conduction band C immediately above the Fermi level is mainly made up of Sr-s and Te-p states. Figure 5 shows the total DOS with the gap energy using PBE-GGA approximation for $x = 0.5$ as prototype.

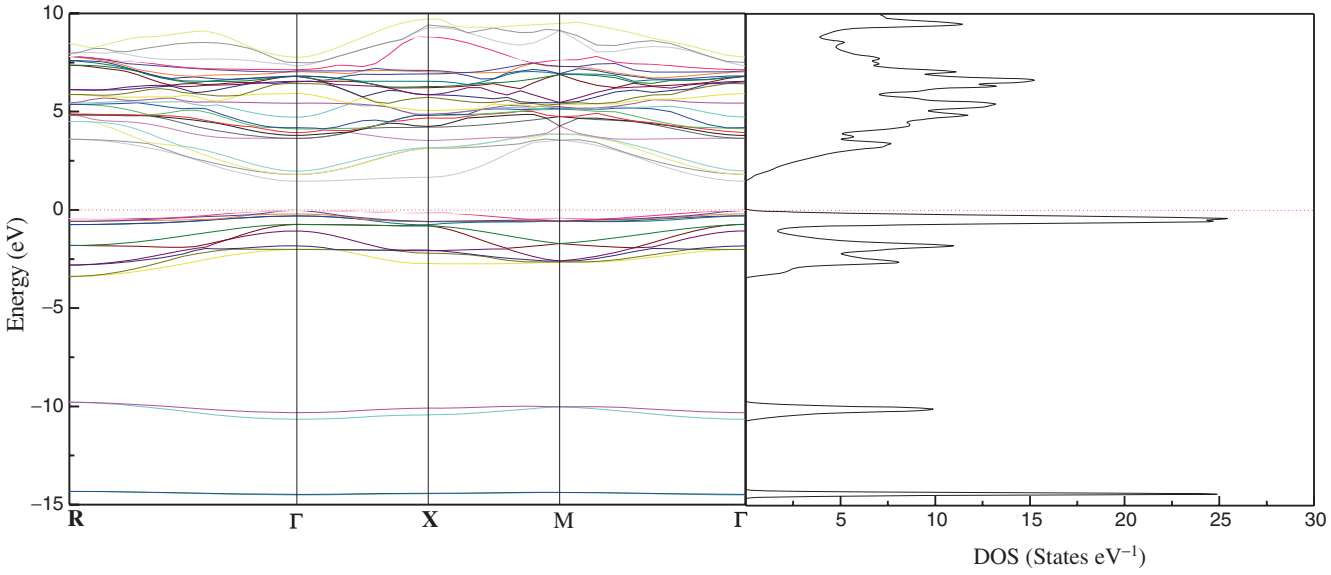

Figure 5. Band structure and projected density of states calculated for $SrTe_{0.5}O_{0.5}$ alloy.

3.3 *Optical properties*

Optical properties of a solid are usually described in terms of the complex dielectric function $\varepsilon(\omega) = \varepsilon_1(\omega) + i\varepsilon_2(\omega)$. The imaginary part of the dielectric function in the long wavelength limit has been obtained directly from the electronic structure calculation, using the joint density of states and the optical matrix elements. The real part of the dielectric function can be derived from the imaginary part by the Kramers–Kronig relation. The knowledge of both the real and the imaginary parts of the dielectric function allows the calculation of important optical functions. The refractive index $n(\omega)$ is given by

$$n(\omega) = \left[\frac{\varepsilon_1(\omega)}{2} + \frac{\sqrt{\varepsilon_1^2(\omega) + \varepsilon_2^2(\omega)}}{2}\right]^{1/2}. \tag{12}$$

At low frequency ($\omega = 0$), we get the following equation:

$$n(0) \approx \varepsilon^{1/2}(0). \tag{13}$$

The refractive index of semiconductors is a very important physical parameter that is related to the microscopic atomic interactions. It represents a fundamental physical aspect that characterizes their optical and electronic properties. Knowledge of the refractive index is essential for devices such as photonic crystals, wave guides, solar cells and detectors [36]. On the other hand, $n(\omega)$ is closely related to the energy band structure of the material. Consequently, many attempts have been made to relate the refractive index and the energy gap E_g through simple relationships [37–42]. However, these relations of $n(\omega)$ are independent of temperature and incident photon energy. The following models are used:

The Moss formula [41] based on atomic model

$$E_g n^4 = k, \tag{14}$$

where E_g is the energy band gap and k a constant. The value of k is 108 eV by Ravindra and Srivastava [38].

Ravindra *et al* [41] have suggested a linear form of n as a function of E_g:

$$n = \alpha + \beta E_g, \tag{15}$$

with $\alpha = 4.084$ and $\beta = -0.62$ eV^{-1}.

To be inspired by a simple physics of light refraction and dispersion, Herve and Vandamme [42] proposed an empirical equation as follows:

$$n = \sqrt{1 + \left(\frac{A}{E_g + B}\right)^2}, \tag{16}$$

with $A = 13.6$ eV and $B = 3.4$ eV.

In the calculations of the optical properties, a dense mesh of uniformly distributed k points is required. Hence, the Brillouin zone integration was performed with 104 and 216 k points in the irreducible part of the Brillouin zone for binary and ternary compounds, respectively. The exchange-correlation potential was treated with the generalized gradient approximation (PBE-GGA).

Using the FP-LAPW method and the three models mentioned above, the refractive index n has been calculated as a function of the percentage oxygen. Our results are depicted in table 4 along with the available experimental data and other theoretical results for the binary compounds, but in the case of alloys, there are no theoretical and experiment values to compare. As compared with the other relations used, it appears that the values of the refractive index obtained from FP-LAPW calculations for the end-point compounds (i.e., SrTe and SrO) are in better agreement with available experimental results.

The refractive indices of solids are strongly connected with their energy band gaps. A correlation between these two

Table 4. Refractive indices of $SrTe_{1-x}O_x$ for different compositions x.

		This work					
	x	FP-LAPW	Relation 14	Relation 15	Relation 16	Exp.	Other calculations
$SrTe_{1-x}O_x$	0	2.448	2.780	2.963	2.796	2.41[a,b]	2.29[c]
	0.25	2.261	2.978	3.233	3.019		
	0.50	2.211	2.923	3.167	2.961		
	0.75	2.143	2.637	2.699	2.613		
	1	1.911	2.385	2.016	2.253	1.80[a,b]	1.943[d], 1.84[e]

[a]Ref [40]; [b]ref [43]; [c]ref [44]; [d]ref [34]; [e]ref [45].

Table 5. Optical dielectric constants of $SrTe_{1-x}O_x$ for different compositions x.

		This work					
	x	FP-LAPW	Relation 14	Relation 15	Relation 16	Exp.	Other calculations
$SrTe_{1-x}O_x$	0	5.993	7.728	8.779	7.818	4.91[a]	6.32[d]
	0.25	5.112	8.868	10.452	9.114		
	0.50	4.889	8.543	10.029	8.767		
	0.75	4.581	6.954	7.285	6.828		
	1	3.651	5.688	4.064	5.076	3.46[b,c]	3.775[e], 3.48[f]

[a]Ref [45]; [b]ref [48]; [c]ref [49]; [d]ref [50]; [e]ref [34]; [f]ref [51].

fundamental properties has significant bearing on the band structure of semiconductors [36,46]. In this study, the fundamental energy band gap of the material of interest increases with increase in the composition x (see table 2), and n decreases with x (see table 4). The ternary alloys show that the smaller band gap material has a larger value of the refractive index as the general behaviour of many other groups III–V semiconductors alloys [47].

The optical dielectric constant was estimated according to equation (13), the results are given in table 5. Our results obtained by the FP-LAPW method are in reasonable agreement with experimental values. Qualitatively, the compositional dependence of the dielectric function of the alloys has the same trend as that of the refractive index. This is not surprising as the dielectric function is directly calculated from equation (13).

3.4 *Thermodynamic properties*

Here we investigate the phase stability of $SrTe_{1-x}O_x$ alloys based on the regular-solution model [52]. The Gibbs free energy of mixing for the alloys is expressed as

$$\Delta G_{\mathrm{m}} = \Delta H_{\mathrm{m}} - T\Delta S_{\mathrm{m}}, \tag{17}$$

where

$$\Delta H_{\mathrm{m}} = \Omega\, x(1-x), \tag{18}$$

$$\Delta S_{\mathrm{m}} = -R\left[x\ln x + (1-x)\ln(1-x)\right], \tag{19}$$

ΔG_{m} and ΔS_{m} are the enthalpy and entropy of mixing, respectively; Ω is the interaction parameter which depends on the material, R the gas constant and T the absolute temperature. The mixing enthalpy of alloys can be obtained as the difference in energy between the alloy and the weighed sum of constituents

$$\Delta H_{\mathrm{m}} = E_{\mathrm{AB}_x C_{1-x}} - xE_{\mathrm{AB}} - (1-x)\,E_{\mathrm{AC}}. \tag{20}$$

The resulting averaged formation enthalpies of alloys are indicated by solid curve in figure 6. ΔH_{m} has a maximum near $x = 0.5$. By rewriting expression (18) as $\Omega = \Delta H_{\mathrm{m}}/x(1-x)$, we can calculate, for each x, a value of Ω from the above DFT values of ΔH_{m}. The only shortcoming we may notice for the regular-solution model for a statistical description of entropy is that the model could be affected by the number of DFT enthalpy values extracted from DFT calculation and, consequently, by the nature of the fit needed. The interaction parameter Ω depending on x is then obtained from a linear fit to the Ω values. The best fit gives

$$SrTe_{1-x}O_x \;\Rightarrow \Omega\ \left(\mathrm{kcal\ mol^{-1}}\right) = 6.47 - 2.34x. \tag{21}$$

The average values of the x-dependent Ω in the range $0 \leq x \leq 1$ obtained from these equations are 5.30 kcal mol^{-1}. Next, we calculate ΔH_{m} expressed by equation (18) with equations (17)–(19), as shown by the solid curve in figure 6. The DFT results of ΔH_{m} (solid circles) are accurately reproduced by the above ΔH_{m} curve. Besides, Ω averaged values independent of x are also used to draw ΔH_{m}, as shown by the dotted curve in figure 6. The latter is symmetric around $x = 0.5$, while the x-dependent parameter is asymmetric, leading to a slight deviation towards the left or right. The effect of this asymmetry will be pronounced in the phase

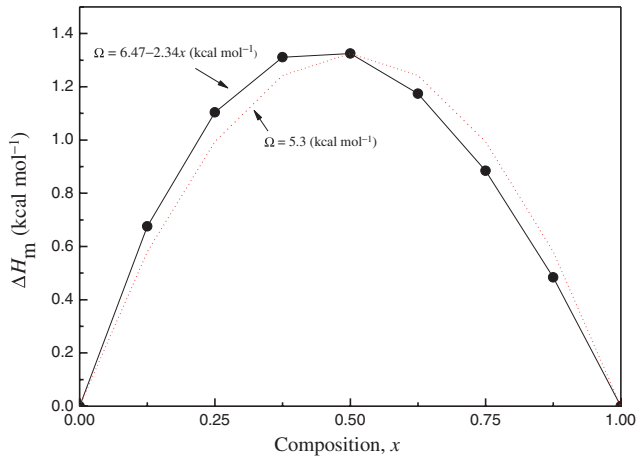

Figure 6. Enthalpy of mixing ΔH_m as function of concentration for $SrTe_{1-x}O_x$ ternary alloy. Solid curve: x-dependent interaction parameters Ω, dotted curve: x-independent interaction parameters Ω.

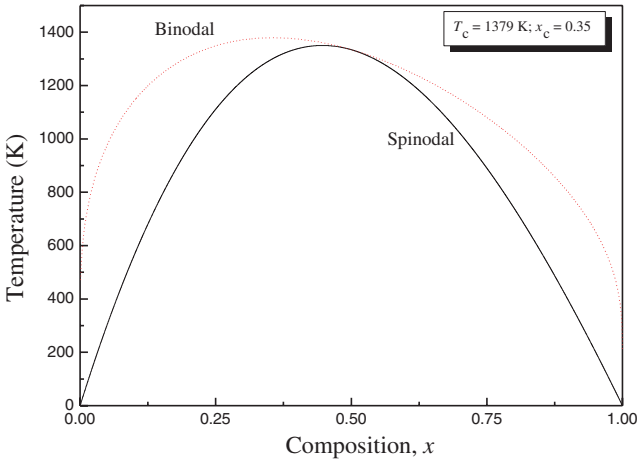

Figure 7. T–x phase diagram of $SrTe_{1-x}O_x$ alloys. Dashed line: binodal curve; solid line: spinodal curve.

diagram shown later. The formation energies are all positive; this implies that the system has strong tendency to segregate in its constituents at low temperature. At high T, disordered configurations are expected to become favoured because of the important increase of the entropic term. Here our aim is to determine the behaviour of the alloy between such limits.

Now, we first calculate ΔG_m by using equations (17)–(19). Then, we use the Gibbs free energy at different concentrations to calculate the $T-x$ phase diagram, which shows the stable, metastable and unstable mixing regions of the alloy. At a temperature lower than the critical temperature T_c, the two binodal points are determined as those points at which the common tangent line touches the ΔG_m curves. The two spinodal points are determined as those points at which the second derivative of ΔG_m is zero; $\partial^2 (\Delta G_m) / \partial x^2 = 0$.

The composition region between two binodal points is the miscibility gap. Thermodynamically unstable phases may exist metastable in cases where the decomposition kinetics is slow, combined with rapid quenching. Within the miscibility gap, there also exists two inflection spinodal points.

Using the x-dependent interaction parameter Ω, we quantitatively determine the critical temperature T_c and the stable and/or metastable boundary lines. In figure 7, we show the resulting phase diagram for alloys of interest. The critical alloy formation temperature occurs at a point where both the first and second derivatives of the free energy are zero, i.e., the plot has no curvature. The miscibility gap disappears at T_c.

We observed a critical temperature T_c equal to 1379 K at the critical composition x_c equal to 0.35. For our phase diagram, more stable semiconductor alloys are likely to form at high temperature; these results indicate that the alloys are unstable over a wide range of intermediate compositions at normal growth temperature.

4. Conclusion

In conclusion, the first-principle calculations were performed to investigate the structural, electronic, optical and thermodynamic properties of $SrTe_{1-x}O_x$ alloys. Results regarding lattice constant and bulk modulus at various compositions x ranging from 0 to 1 are reported and compared where possible with the available experimental and theoretical data in the literature. It is shown that the use of WC-GGA in our calculations is more appropriate than PBE-GGA and LDA and gives a good description of structural properties such as lattice parameters and bulk modulus. Our calculations showed that the lattice constant, bulk modulus, band gap and refractive index were found to depend nonlinearly on alloy composition x. Finally, the enthalpy of mixing ΔH_m is calculated in the whole composition range. The calculated ΔH_m is expressed within the regular-solution model using the x-dependent interaction parameter Ω. The calculated phase diagram indicates a significant phase miscibility gap. These results indicate that the ternary alloys are unstable over a range of intermediate composition.

References

[1] Nakanishi Y *et al* 1992 *Appl. Surf. Sci.* **66** 515
[2] Abtin L and Springholz G 2008 *Appl. Phys. Lett.* **93** 163102
[3] Rack P *et al* 1998 *J. Appl. Phys.* **84** 3676
[4] Asano S *et al* 1978 *Phys. Status Solidi B* **89** 663
[5] Zimmer H G *et al* 1985 *Phys. Rev. B* **32** 4066
[6] Khenata R *et al* 2003 *Physica B* **339** 208
[7] Shameen Banu I *et al* 1998 *J. Low Temp. Phys.* **112** 211
[8] Pietro Cortona 2004 *Int. J. Quant. Chem.* **99** 828
[9] Rached D *et al* 2004 *Phys. Status Solidi B* **241** 2529
[10] Marinelli F and Lichanot A 2003 *Chem. Phys. Lett.* **367** 430
[11] Straub G K and Harrison W A 1989 *Phys. Rev. B* **39** 10325

[12] Liwei Shi *et al* 2011 *Physica B* **406** 181
[13] Chaudhary V *et al* 1998 *J. Catal.* **178** 576
[14] Chen G *et al* 1998 *Science* **280** 1913
[15] Duffy T S and Ahrens T J 1995 *J. Geophys. Res.* **100** 529
[16] Jackson (ed.) 1982 *High pressure research in geophysics* (Tokyo, Japan: Center for Academic Publications) p 93
[17] Yoneda A 1990 *J. Phys. Earth* **38** 19
[18] Pandey *et al* 1991 *Phys. Rev. B* **43** 9228
[19] Vegard L 1921 *Z. Phys.* **5** 17
[20] Zunger A *et al* 1990 *Phys. Rev. Lett.* **65** 353
[21] Hohenberg P and Kohn W 1964 *Phys. Rev. B* **136** 864
[22] Kohn W and Sham L J 1965 *Phys. Rev. A* **140** 1133
[23] Blaha P *et al* 2001 WIEN2k, An augmented plane wave plus local orbitals program for calculating crystal properties (Vienna, Austria: Karlheinz Schwarz, Techn. Universitat)
[24] Perdew J P and Wang Y 1996 *Phys. Rev. B* **45** 13244
[25] Perdew J P *et al* 1996 *Phys. Rev. Lett.* **77** 3865
[26] Wu Z and Cohen R E 2006 *Phys. Rev. B* **73** 235116
[27] Engel E and Vosko S H 1993 *Phys. Rev. B* **47** 13164
[28] Tran F and Blaha P 2009 *Phys. Rev. Lett.* **102** 226401
[29] Becke A D and Johnson E R 2006 *J. Chem. Phys.* **124** 221101
[30] Syassen K *et al* 1987 *Phys. Rev. B* **35** 4052
[31] Baltache H *et al* 2004 *Physica B* **344** 334
[32] Dufek P *et al* 1994 *Phys. Rev. B* **50** 7279
[33] Jochen Heyd *et al* 2005 *J. Chem. Phys.* **123** 1
[34] Ghebouli M A *et al* 2011 *J. Alloys Compd.* **509** 1440
[35] Bernard J E and Zunger A 1986 *Phys. Rev. B* **34** 5992
[36] Ravindra N M *et al* 2007 *Infrared Phys. Technol.* **50** 21
[37] Moss T S 1950 *Proc. Phys. Soc. B* **63** 167
[38] Gupta V P and Ravindra N M 1980 *Phys. Status Solidi B* **100** 715
[39] Ruoff A L 1984 *Mater. Res. Soc. Symp. Proc.* **22** 287
[40] Reddy R R *et al* 1993 *Infrared Phys.* **34** 103
[41] Ravindra N M *et al* 1979 *Phys. Status Solidi B* **93** 155
[42] Herve J P L and Vandamme L K J 1994 *Infrared Phys. Technol.* **35** 609
[43] Moss T S *et al* 1973 *Semiconductor opto-electronics* (London: Butterworths)
[44] Salem M A 2003 *Chin. J. Phys.* **41** 288
[45] Lines M E 1990 *Phys. Rev. B* **41** 3372
[46] Bouarissa N and Boucenna M 2009 *Phys. Scr.* **79** 015701
[47] Adachi S 1987 *J. Appl. Phys.* **61** 4869
[48] Galtier M 1972 *J. Phys. Chem. Solids* **33** 2295
[49] Sangster M J L *et al* 1970 *J. Phys. C* **3** 1026
[50] Dadsetani M and Pourghazi A 2006 *Phys. Rev. B* **73** 195102
[51] Eric J Wu and Ceder G 2001 *J. Phys.* **89** 15
[52] Swalin R A 1961 *Thermodynamics of solids* (New York: Wiley)